An analysis of regional climate model performance over the tropical Americas. Part I: simulating seasonal variability of precipitation associated with ENSO forcing

By ETIENNE TOURIGNY and COLIN G. JONES*†, *Université du Québec à Montréal, CRCMD Network, Montréal, Canada*

ABSTRACT

Sea surface temperature (SST) anomalies associated with El Niño/Southern Oscillation (ENSO) constitute a major source of predictability in the tropics. We evaluate the ability of a regional climate model (the Rossby Centre Atmospheric Model; RCA) to downscale SST and large-scale atmospheric anomalies associated with ENSO. RCA is configured over the tropical east Pacific and tropical Americas and runs for the period 1979–2005, using European Centre for Medium-Range Weather Forecasts (ECMWF) lateral and surface boundary conditions. We study the ability of RCA to represent regional patterns of precipitation, with respect to both the climatology and interannual variability associated with ENSO. The latter is achieved by grouping the simulations into El Niño and La Niña composites and studying the delayed response of precipitation to SST forcing in four regions of Central and South America.

In this paper, we concentrate on seasonal mean timescales. We find that RCA accurately simulates the main features of the precipitation climatology over the four regions and also reproduces the majority of the documented regional responses to ENSO forcing. Furthermore, the model captures the variability in precipitation anomalies between different ENSO events. The model exhibits a wet bias over the northern Amazon and slightly overestimates the magnitude of ENSO anomalies over Central America.

1. Introduction

The branch of climate prediction known as seasonal forecasting fills a gap between short-range weather forecasting and climate prediction. Seasonal forecasting aims to make useful predictions of climate anomalies on timescales of about 1 month to 1 yr. The benefits of seasonal prediction are multiple, ranging from disaster prevention (floods and droughts) to resource planning (agriculture and energy). Past studies have established a potential predictive skill on seasonal timescales in tropical regions (Goddard et al., 2001, and references therein). The main source of this predictability stems from forcing of large-scale atmospheric circulation anomalies by tropical sea surface temperature (SST) anomalies. These SST anomalies (SSTAs) evolve on relatively slow timescales, increasing atmospheric predictability beyond that normally associated with unforced atmospheric

motions (Shukla, 1998). The coupled ocean–atmosphere phenomenon known as the El Niño/Southern Oscillation (ENSO) is the leading mode of interannual SST variability in the tropics (Wang et al., 1999), hence SSTAs associated with ENSO constitute a major source of potential predictability on seasonal timescales, particularly in tropical regions (Goddard et al., 2001).

Coupled ocean-atmosphere general circulation models (CGCMs) can simulate with reasonable accuracy the evolution of tropical SSTAs on seasonal timescales associated with ENSO (Latif et al., 1998; Palmer et al., 2004). Atmosphere only GCMs (AGCMs) can then be forced either with these predicted SSTAs or with persisted observed SSTAs, to assess their impact on important meteorological variables. Atmosphere only GCMs have some skill in simulating the response of the large-scale tropical atmospheric circulation to anomalous SST forcing (Philander, 1990; Shukla et al., 2000). Nevertheless, users of seasonal predictions often require localized information on regional climate anomalies, hence some means of downscaling GCM simulated large-scale anomalies is required, to maximize the utility of these seasonal forecasts. Regional climate models (RCMs), through their increased resolution, offer one means of downscaling GCM

*Corresponding author.
e-mail: colin.jones@smhi.se
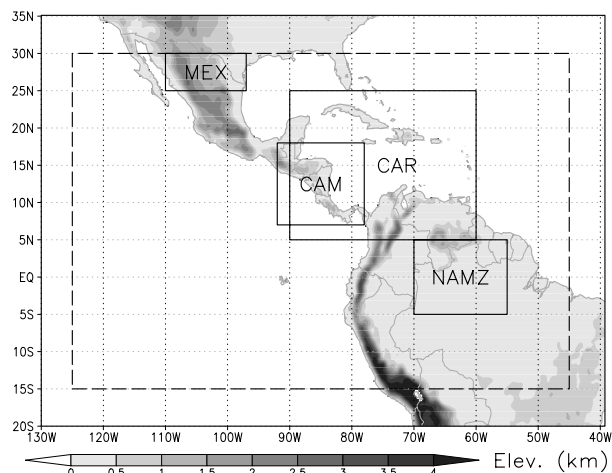†Now at: SMHI, Rossby Centre, SE-601 76, Norrköping, Sweden.

Fig. 1. Domain of the study and chosen regions. The dashed box shows the area of analysis.

seasonal predictions to the scale more suited to end-users (Sun et al., 2006).

This study covers areas of the tropical Americas such as Mexico, Central America, the Caribbean and northern South America as well as the tropical east Pacific and north Atlantic oceans (see Fig. 1). A number of studies have linked east Pacific and tropical Atlantic SSTAs to precipitation anomalies in the Caribbean and northern South America (Goddard et al., 2001). The tropical North Atlantic (TNA) SSTAs are due to both ENSO teleconnections and local variability, and the relative contribution to precipitation variability of these two water basins is somewhat difficult to ascertain (Enfield and Alfaro, 1999; Giannini et al., 2000; Taylor et al., 2002). Over Mexico and Central America, the response to anomalous SST forcing is somewhat weaker than over South America yet clearly present (Ropelewski and Halpert, 1987; Enfield, 1996; Enfield and Mayer, 1997; Giannini et al., 2000; Magaña et al., 2003).

Over South America, a GCM has been used successfully by Centro de Previsão de Tempo e Estudos Climáticos (CPTEC) for operational seasonal prediction over South America (Marengo et al., 2003) for a number of years. The use of RCMs (RegCM3 and EtaClim) has indicated an improvement in seasonal prediction of precipitation in regions of Brazil, such as the Amazon (Chou et al., 2005) and Nordeste (Sun et al., 2006), as a result of dynamical downscaling. In other studies, the same RCMs provide a fairly accurate simulation of precipitation over South America, both in terms of the mean climatology and anomalies during ENSO events (Fernandez et al., 2006a,b; Seth et al., 2007). Existing RCM studies covering Central America and the Caribbean are scarce. In Xie et al. (2007), the ROAM regional ocean–atmosphere model reproduces the main climatological features of the tropical east Pacific and shows an improvement in the simulation of mesoscale features due to its increased resolution. A study by Hernandez et al. (2006) describes a simulation using the MM5 RCM over Central America. Variables

such as temperature, wind speed and water vapour mixing ratio were well simulated, but discrepancies in simulated precipitation were attributed to the use of only two seasonal maps of land cover. The North American Monsoon (also defined as the Mexican Monsoon) described in Adams and Comrie (1997), is centred over northwestern Mexico and has been covered by numerous RCM studies. The MM5 RCM can reproduce the climatological features of the North American Monsoon (Xu et al., 2004) and sensitivity tests to convective schemes indicate improved performance using the Kain–Fritsch scheme (Gochis et al., 2002).

In this set of experiments, we use an RCM to downscale so-called perfect boundary conditions as defined by European Centre for Medium-Range Weather Forecasts (ECMWF) analysed lateral and surface boundary conditions. This is done to assess the ability of an RCM to generate small-scale regional detail with respect to ENSO forced anomalies, given accurate large-scale forcing. Subsequent to a successful evaluation of the RCM downscaling ability forced by analysed boundaries, the logical next step is to force the same RCM with boundary conditions derived from an atmospheric or coupled GCM. This step is deferred to a future study. In this study, we run the Rossby Centre Regional Atmospheric Model version 3 (referred to as RCA) (Jones et al., 2004; Kjellström et al., 2005), with observed SSTs and analysed lateral boundary conditions (LBCs) for the period 1979–2005. The model was configured to cover the tropical east Pacific and tropical Americas and run at a resolution of $0.33°$ for most of our analysis. As $0.33°$ is significantly higher resolution than is generally employed by GCMs in seasonal prediction, we would also like to more directly assess the benefits of increased resolution with respect to simulating ENSO precipitation variability. To achieve this, we have conducted an additional set of experiments using the same RCA at a resolution of $1°$, the approximate resolution of both the ECMWF analysis and operational GCMs currently in use for seasonal prediction. Comparison between the RCA $0.33°$ and $1°$ integrations will indicate benefits accruing directly from improved resolution. Figure 1 shows the entire model domain, while the inner dashed box shows the area of analysis (excluding the outer 15 points of the model). An assessment is made of the model's ability to simulate regional-scale anomalies associated with either El Niño or La Niña conditions. This paper looks at regional-scale variability associated with ENSO at seasonal mean timescales. Our primary emphasis is on precipitation anomalies as these have the largest impact on society. Part II of this study (Tourigny and Jones, 2009), hereafter referred to as TJ2009b, looks at subseasonal timescale precipitation.

2. Model and data

2.1. Domain of study and regions

The domain of study comprises Central America and most of the tropical regions of the Americas. The RCM domain includes the

main area of the east Pacific Inter Tropical Convergence Zone (ITCZ). Convective anomalies over this region, associated with ENSO SST variability, are the main forcing term of large-scale atmospheric circulation anomalies that subsequently influence Central and South America. Hence, the majority of the anomalous atmospheric convection over the equatorial east Pacific and associated circulation anomalies are simulated within the RCM domain. The strong surface forcing in equatorial regions along with the relatively large model domain mean the RCM is less strongly constrained by the lateral (atmospheric) LBCs than in typical mid-latitude RCM integrations.

Referring to Fig. 1, the regions where we evaluate the model's ability to simulate regional-scale climate anomalies are: MEX (northern Mexico, 25°N–30°N, 110°W–97°W), CAR (Caribbean, 5°N–25°N, 90°W–60°W), CAM (Central America, 7°N–18°N, 92°W–78°W) and NAMZ (northern Amazon, 5°S–5°N, 70°W–55°W). These regions have been chosen based on previous studies which identify regions of ENSO-related precipitation variability. Details of the observed precipitation associated with ENSO variability and the mechanisms forcing this variability, as well as relevant references, are discussed in Section 4.1.

2.2. Model setup

RCA uses the Kain–Fritsch convection scheme (Kain and Fritsch, 1990, 1993; Kain, 2004) for representing both deep and shallow convection. Deep convection uses a CAPE consumption closure, while shallow convection is assumed to consume subcloud layer turbulent kinetic energy (TKE) within a given time period (Deng et al., 2003). Isotropic subgrid scale turbulence is represented by a moist TKE scheme (Cuxart et al., 2000; Lenderink and Holtslag, 2004). Resolved scale clouds are parametrized following the approach of Xu and Randall (1996), while a diagnostic shallow cumulus cloud fraction follows Albrecht (1981). A cloud fraction associated with parametrized deep convective up and downdrafts is diagnosed as a function of the convective mass-flux, following Xu and Krueger (1991). Large-scale condensation uses the scheme due to Rasch and Kristansson (1998), while the RCA radiation scheme is described in Savijärvi (1990) and Räisänen et al. (2000). The land surface is comprised of three active soil layers and is documented in Samuelsson et al. (2006). Surface and subsurface physiography is prescribed each month using the high-resolution ECOCLIMAP global data set (Masson et al., 2003), which provides monthly climatological values. The model uses the Davies (1976) boundary relaxation technique with an eight-point relaxation zone for adjusting the interior RCM solution towards the prescribed lateral values.

Initial and lateral boundary conditions were obtained from observed SSTs and ECMWF ERA-40 reanalyses (Uppala et al., 2005). After August 2002 LBCs were derived from the ECMWF

operational analysis. For all years covering the period 1979–2005, RCA is run for one calendar year with observed SSTs and analysed LBCs. Soil temperature and moisture values are initialized from the ECMWF analysed values relevant for the calendar month (December) of each year used as initial conditions. While we recognize that deep soil moisture spins up on much longer timescales than 13 months, the procedure employed here is done to mimic actual seasonal forecasting using a quasi-observed soil moisture field and in terms of computational cost. Experiments on soil moisture reinitialization show that frequent reinitialization increases short-term (on the order of weeks) accuracy (Qian et al., 2003), and suggest a minimal importance of soil moisture memory (Pan et al., 1999). Moreover, continuous reinitialization removes possible drift in soil moisture due to systematic errors in the RCM formulation (Qian et al., 2003).

In this study, we employ only one RCM integration, per 13 month period, to define the simulated precipitation for that year. In a true GCM–RCM prediction system, an ensemble of GCM simulated LBCs would be required to better quantify the statistical robustness of any RCM simulated precipitation anomalies. In this manner, variability in the simulated LBCs (both with respect to differing GCMs and the natural variability as simulated by a single GCM) would be included in the final estimate of GCM–RCM precipitation anomalies. Here, we use a hindcast approach, with analysed LBCs applied to the RCM. This we believe reduces the need to sample a variety of LBCs, although we recognize that a similar exercise with another global reanalysis data set might help to strengthen this assertion. Unfortunately this level of computation was beyond the scope of this study and must be deferred to later efforts. Similarly, for a true GCM–RCM prediction system, a variety of RCMs would allow a better estimate of the statistical robustness of simulated regional responses to a given LBC data set. Again application of a suite of RCMs is beyond the scope of this study.

The final step in establishing the statistical robustness of RCM precipitation anomalies is to ask, for a given LBC data set and RCM what is the RCM internal variability on 3–12 months lead times? To assess this, we constructed a five member ensemble of RCA simulations for the El Niño year of 1983, whereby RCA was initialized progressively 1 d later in the period 1–5 December 1982. Each RCA simulation used the same LBC and SST data set and was run to the end of December 1983. Analysis of the simulated precipitation in this five member ensemble indicated that the major regional-scale anomalies were very similar across all members, suggesting the control exerted by the (anomalous) SST and large-scale atmospheric circulation, as defined by the applied LBCs, limits the degree of variability internal to the RCM domain. This argument holds most strongly for the stronger ENSO events which are the main emphasis of this work.

2.3. Observations

The emphasis of this study is on precipitation variability due to its large societal impact. Sea level pressure (SLP), low-level (925 hPa) wind, as well as upper-level (250 hPa) geopotential height and wind are also studied to better understand the dynamics of the atmospheric circulation anomalies controlling the regional patterns of anomalous precipitation.

Satellite observations offer the most spatially and temporally complete estimate of observed precipitation. The highest resolution observation is the Tropical Rainfall Measuring Mission (TRMM) product 3B43 (Huffman et al., 2007), available at a resolution of $0.25°$ and derived from satellite and in situ observations. TRMM 3B43 is only available from 1998 to present, this period does not include a sufficient number of ENSO events for a robust analysis of the simulated ENSO forced variability. Version 2 of the Global Precipitation Climatology Project (GPCPv2) gives monthly estimates of precipitation on a grid of $2.5°$ resolution, from 1979 to present (Adler et al., 2003). These observations are at a coarser resolution than the model ($2.5°$ vs. $0.33°$), therefore a more precise gridded product is required for land areas. We choose the Climatic Research Unit's TS 2.1 $0.5°$ global land data set, covering the period 1901–2002 (Mitchell and Jones, 2005). An additional quasi-observation is given by the ECMWF ERA-40 reanalysis available for 1957–2002, as well as ECMWF operational analysis from August 2002, from which we obtain precipitation, SLP, geopotential height and wind vector estimates. The resolution of ERA-40 and ECMWF is T106 ($\sim1°$ at the equator), although all variables excluding precipitation were obtained at $2.5°$ resolution. The reader is reminded that ECMWF is also used as an LBC for the regional model, allowing an estimate of the 'added value' of the RCM compared to the driving data set. We refer to these data sets respectively as TRMM, GPCP, CRU and ECMWF. From these data sets, we evaluate the model's climatology and interannual variability for the 1979–2001 period. TRMM is used to evaluate the model performance for the 1998–2005 period, with an emphasis on high-resolution regional patterns. In particular, we focus on regional scale, seasonal mean precipitation anomalies associated with El Niño and La Niña conditions.

3. Climatology

3.1. Methodology

The first step in our evaluation is to assess the simulated precipitation climatology over the regions of interest. While in principle interannual anomalies associated with ENSO can still be simulated by a model that fails to accurately simulate the regional climatology, the propagation and development of remote ENSO teleconnections is often sensitive to details of the background climatology (Simmons et al., 1983; Sardeshmukh and Hoskins, 1988). Furthermore, an accurate representation of the climato-

logical conditions increases our confidence that the model correctly simulates key regional climate processes. We first evaluate the seasonal mean SLP and precipitation, concentrating on the boreal winter (JFM) and summer (JAS) seasons. Second, we plot annual cycle time-series of spatially averaged precipitation, for land points only, for each of the regions shown in Fig. 1.

3.2. Results

3.2.1. Seasonal averages. Figure 2 shows the climatological mean SLP and 925 hPa winds (left-hand column) and 250 hPa geopotential height and winds (right-hand column) for seasons JFM and JAS (averaged for 1979–2001) from ECMWF and RCA. Figure 3 gives the climatological seasonal mean precipitation for the same seasons and period, here GPCP, CRU, ECMWF and RCA are presented.

Season JFM (Figs 2a–d and 3, left-hand column) shows a relative minimum in observed precipitation on the equator in the east Pacific ITCZ, which is mainly captured by the model, with a small positive bias compared to GPCP. The minimum simulated over northern South America is realistic, although the maxima in the southern Amazon and the Atlantic ITCZ are somewhat excessive. ECMWF precipitation is excessive over most of the domain except over the southern Amazon, where precipitation is underestimated. It is worth noting that the excessive precipitation simulated by RCA close to its eastern boundary in the Atlantic ITCZ is also evident in the ECMWF results. This may suggest a strong and perhaps erroneous forcing of the RCA precipitation by the adjacent ECMWF atmospheric boundary conditions. Upper-level geopotential and wind vectors show a maximum in geopotential height over the southern portion of the RCA domain and the presence of the subtropical jet over the northern portion of the domain, accurately simulated by RCA.

Over the Amazon region in JFM season, the low-level wind field in RCA is clearly stronger than in ECMWF (Figs 2a and c). This stronger wind field is consistent with the higher rainfall rates in RCA over the Amazon region during JFM compared to ECMWF (Figs 3e and g). We are unable to determine if the excessive precipitation in RCA (and associated diabatic heating) causes the excessive low-level wind speeds in RCA, or if the wind speed bias and associated convergence of moisture into Amazonia drive an erroneous response in the convection scheme. Compared to GPCP and CRU observations, the RCA precipitation is excessive in this region while ECMWF precipitation is biased low. We are unable to evaluate the accuracy of the ECMWF low-level winds in this region, but through a balanced thermal-dynamics argument one might conclude that the 'true' low-level wind speed is therefore somewhere between the ECMWF and RCA values.

In season JAS (Figs 2e–h and 3, right-hand column), GPCP precipitation and ECMWF SLP and winds indicate that the ITCZ has migrated to $\approx10°$N in the eastern Pacific and western
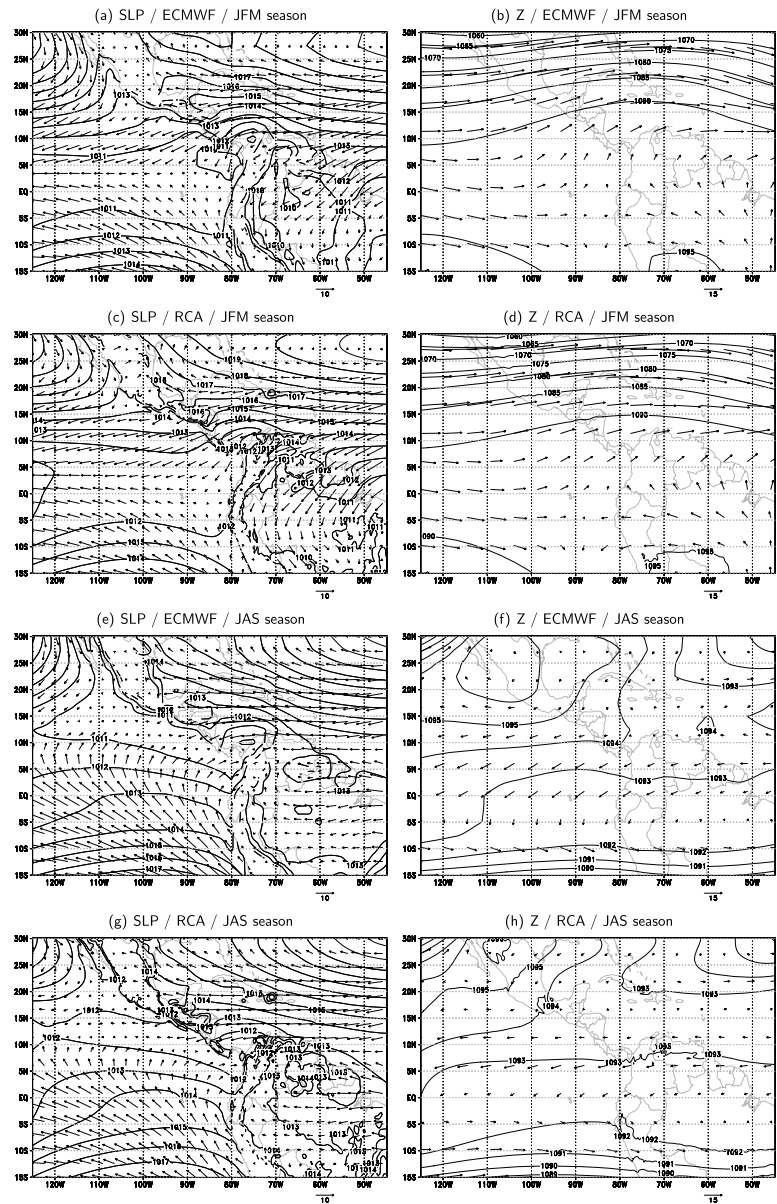
Fig. 2. Climatological SLP (contours in hPa) and 925 hPa winds (vectors in m s^{-1}) in left-hand column, 250 hPa geopotential height (contours in dam) and winds (vectors in m s^{-1}) in right-hand column. The scale of the wind vectors is indicated on each figure.

Atlantic, with a significant strengthening of the east Pacific ITCZ. This migration and intensification, accompanied by a northward-displacement of maximum 250 hPa geopotential height, is largely captured by the model. A clear coastal precipitation minimum is correctly simulated by RCA along the west coast of South America in JAS, while precipitation rates associated with the North American Monsoon are also accurate, with the Mexican Monsoon penetrating to $\approx 27°$N along the west coast. The main area of disagreement lies in the more rapid decrease in precipitation in the observations as one moves south of the Amazon region in South America. RCA simulates a number of regional precipitation patterns that are spatially supported by the CRU observations. In this region, the actual observation

data going into the CRU data set are uncertain and may not be actually representative of 0.5° resolution. Hence, it is difficult to evaluate the simulated regional details without an improved observational data set. RCA reproduces most of the spatial structure of precipitation in JAS, although of higher intensity in some areas. In Section 5, we will show that this higher intensity is comparable to the higher-resolution TRMM data.

Regions of high SLP over the oceans generally correspond to the descending branches of the Hadley Cell and are coincident with extreme dry conditions. In RCA, the SLP field is well structured with the minimum SLP well located and a clear northward extension of the ITCZ in JAS into Mexico, coincident with the North American Monsoon. The SLP values over the Atlantic and
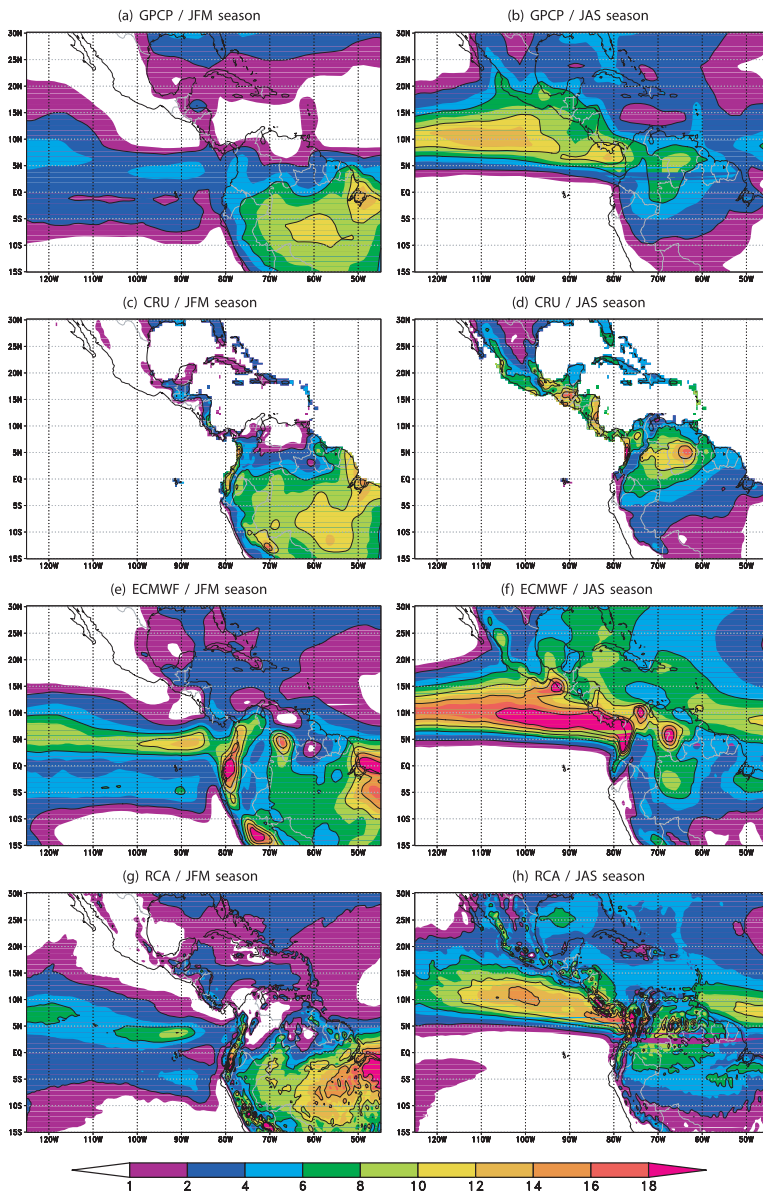
South America are also generally accurate. There is, however, a positive SLP bias of ≈1 hPa in the east Pacific, particularly in the ITCZ region. The ECMWF climatological precipitation for JAS shows a clear overestimate in the Pacific ITCZ. In the tropics, diabatic heating associated with precipitation and surface SLP are dynamically related. In a free-running model (i.e. one not constrained by the assimilation of observations), a positive precipitation bias such as in ECMWF might be expected to be associated with a low-pressure bias in the ITCZ. In ECMWF, this relationship is not necessarily present, as the assimilation of SLP observations can bring the analysed SLP back towards observed values even while the atmospheric diabatic heating is overestimated. To partially evaluate the ECMWF SLP field, we

also analysed SLP and precipitation from the Japanese Reanalysis (JRA25; Onogi et al., 2007). The JRA25 precipitation values in the east Pacific ITCZ are less than in ECMWF (although still higher than satellite values), but the JRA25 and ECMWF SLP fields are quite similar (not shown). We therefore conclude that the assimilation process likely constrains SLP in ECMWF and the RCA ≈1 hPa bias is a genuine model error.

3.2.2. Annual cycle. In Fig. 4, we plot the climatological mean annual cycle of precipitation (years 1979–2001) for the four separate regions outlined in Fig. 1. On the *x*-axis of the plots, we indicate the typical rainy season duration. Figure 4a shows results for the CAR region, where RCA reproduces the annual cycle and seasonal transitions, mostly within the range
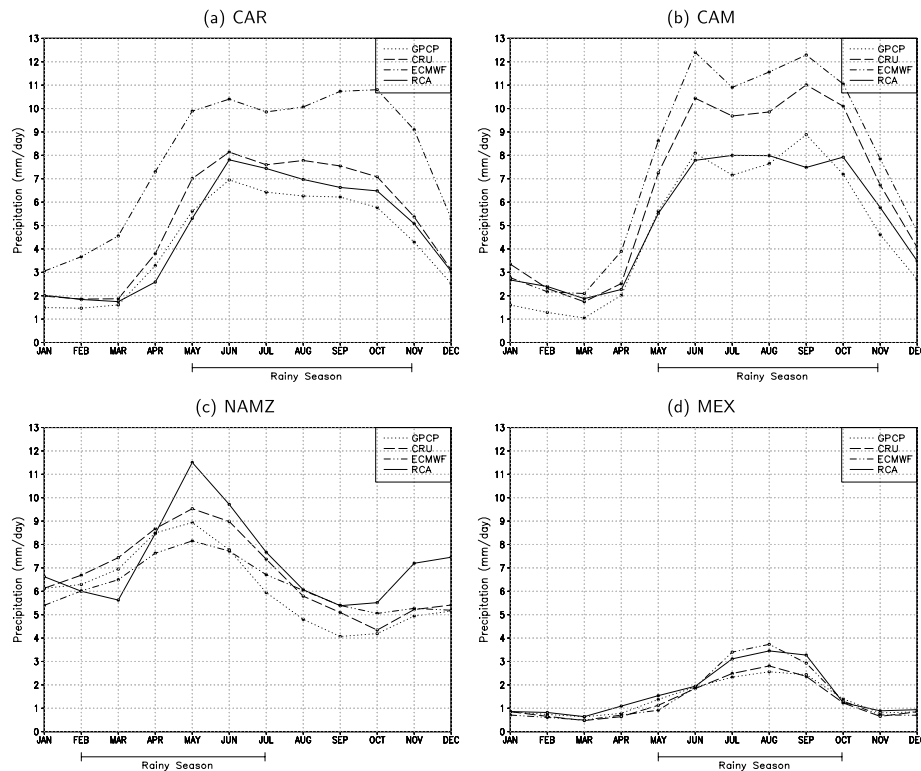
Fig. 4. Spatial mean climatological precipitation over land, annual cycle by region. The duration of the climatological rainy season is indicated for each region on the *x*-axis.

of GPCP and CRU observations. ECMWF values are excessive in this region and cannot be used as an observational surrogate. Figure 4b shows the CAM region, where RCA follows the GPCP estimates quite closely. CRU and GPCP over the CAM region differ by up to 2 mm d^{-1} in the rainy season (May–October).

Close inspection of the rainy season reveals a well-documented feature of precipitation in Central America: the midsummer drought (MSD), when there is a relative minimum of precipitation in July–August in the middle of the rainy season (Magaña et al., 1999; Alfaro, 2002; Magaña and Caetano, 2005; Taylor and Alfaro, 2005; Small et al., 2007). RCA fails to represent this feature in the climatological spatial average over CAM. To investigate this problem further, Fig. 5 shows the climatological average of July and August rainfall minus the average for June and September over the entire model domain. The same method is used in Small et al. (2007), wherein it is shown that the MSD is initiated by the northward migration of the east Pacific ITCZ and the westward expansion of the Atlantic subtropical high. These changes in SLP induce low-level divergence and subsidence over Central America, and the circulation changes due to the precipitation deficit induce a low-level anticyclonic flow over the Gulf of Mexico, with subsequent drying. In RCA, SLP and low-level wind changes in July, relative to June, are negligible in the Caribbean, whereas ECMWF

shows increased northeasterlies and divergence (not shown), which explains the precipitation deficit in the western Caribbean (Fig. 5c). However, both ECMWF and RCA show a precipitation deficit on the west coast of Central America (north of Costa Rica), consistent with divergence and subsidence. Moreover, all data sets agree on the dry anomaly over the Gulf of Mexico (although slightly overestimated by RCA). The precipitation increase over western Mexico (part of the Mexican Monsoon) is also well simulated by RCA. There is evidence, both in model and observations, of a precipitation increase on the east coast of Central America, due to the increased easterlies associated with orographic forcing. RCA does therefore appear to simulate the MSD over the western part of Central America, but incorrectly simulates a wet anomaly in the western Caribbean, as a result the MSD is absent in the spatial average of the CAM region. Nevertheless, specific land-based negative and positive anomalies in the July and August precipitation relative to the June and September amounts are well captured by RCA over central America (see Fig. 5d). The primary problem related to the simulation of the MSD appears to be associated with an incorrect response over the west Caribbean Sea. Further analysis is required to fully understand this incorrect response.

Over the NAMZ region (Fig. 4b), the rainy season extends from February to July and the seasonal variation is of smaller
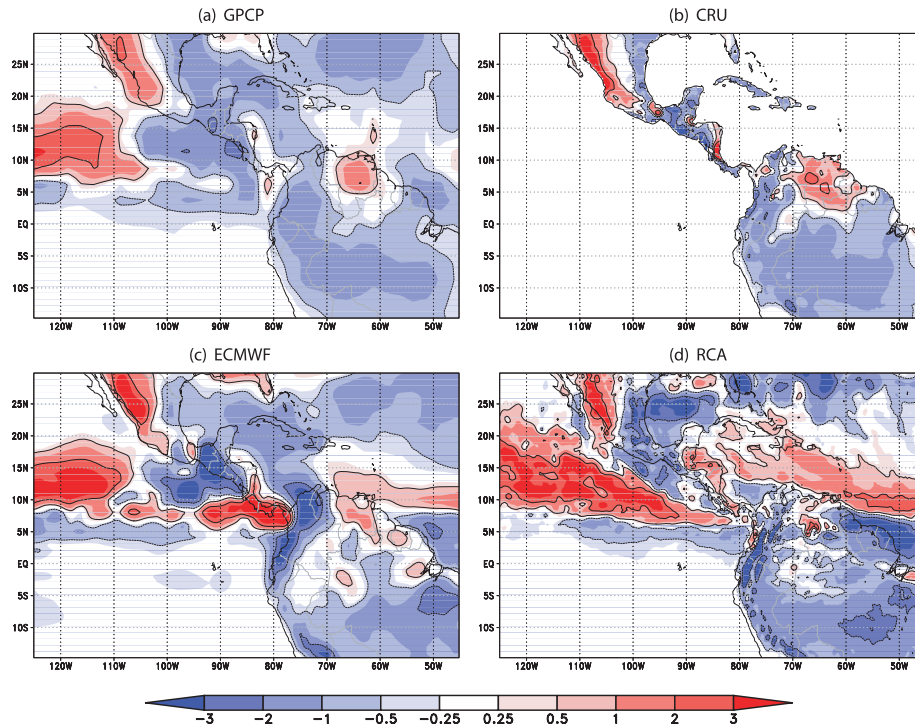
Fig. 5. Climatological average of July and August minus the average of June and September precipitation (mm d^{-1}).

amplitude. The model is generally wetter than observed, but the timing of the rainy season is reasonably captured. Moist conditions extend too long into the OND season, with an unrealistic secondary maximum in December. This is similar to many models which produce a secondary peak in precipitation associated with the semi-annual cycle of solar forcing at the equator (Rauscher et al., 2007; Seth et al., 2007). A continuous 3-yr integration has shown that this is not a problem related to spin-up of soil moisture with the biannual peak in precipitation evident in all 3 yr of this run. ECMWF precipitation intensity is closer to observations, however the amplitude of the seasonal variations is underestimated. The MEX region (Fig. 4c) is far drier, exhibiting a weak rainy season from May to September. The timing of the rainy season is well reproduced by the model, however there is a slight wet bias ($\sim$1 mm d^{-1}) during that period which is also present in ECMWF.

In this section, we have shown that RCA simulates the climatological precipitation with some degree of accuracy both over the east Pacific and adjacent land regions. The model successfully captures a number of regional details, giving some confidence it simulates the majority of the important processes controlling precipitation over the tropical Americas and eastern Pacific. A more detailed evaluation of small-scale regional precipitation details is deferred until section 5 where we employ the TRMM data set for the shorter 1998–2005 period. In the next section, we evaluate the simulated precipitation variability in response to prescribed ENSO SST forcing.

4. Interannual variability

4.1. A review of ENSO effects and teleconnections

During the warm phase of ENSO (El Niño), anomalously warm waters are located in the central and east Pacific with a general weakening of the climatological east-west SST gradient. In the cold phase of ENSO (La Niña), central and east Pacific SSTs are anomalously cold with a concomitant increase in the longitudinal SST gradient. In El Niño events, warm SSTAs lead to anomalous deep convection in the central and east Pacific (Philander, 1990). Through atmospheric and oceanic teleconnections, other regions of the globe experience anomalies in rainfall and temperatures in response to this anomalous Pacific convection (Alexander et al., 2002). Studies by Ropelewski and Halpert (1987, 1996) identify regional-scale patterns associated with El Niño (warm ENSO) events through the study of composites representing years (−), (0) and (+), which are the years before, during and after a 'typical' ENSO event, with the peak of anomalous SST in the OND(0) season (i.e. October–December of year (0)).

Anomalous precipitation patterns documented over our domain of study associated with El Niño conditions are (1) wet anomalies over the Gulf of Mexico and northern Mexico from October (0) to March (+); (2) dry conditions over Central America and the Caribbean from July to October (0); (3) dry conditions over northeastern South America from July (0) to March (+). The regional patterns for La Niña are, in a general

sense, opposite signed anomalies to El Niño (Aceituno, 1988; Ropelewski and Halpert, 1989), therefore subsequent analysis will concentrate on the warm El Niño events, with some minor verification that the model simulates correctly the opposite signed La Niña anomalies.

The mechanisms thought to induce precipitation anomalies related to El Niño are multiple. During the summer of year (0), as the SSTA is becoming established, anomalous convection over the east Pacific modifies the Walker and Hadley circulations, with increased subsidence and decreased rainfall in the Caribbean (Chiang et al., 2000). The reduction in SLP over the tropical east Pacific and increase over the North Atlantic (which strengthens the trade winds) implies low-level divergence over the Caribbean Sea and convergence in the tropical east Pacific. This is responsible for a decrease in moisture convergence, and thus precipitation, over Central America and the Caribbean (Giannini et al., 2000, 2001b). The anomalous Walker Cell is also thought to be responsible for increased subsidence and decreased rainfall over the Amazon and northeast Brazil (Kousky et al., 1984).

A chain of teleconnections known as the 'Atmospheric Bridge' (Alexander et al., 2002) is thought to regulate the delayed responses to ENSO throughout much of the study area. Anomalous tropospheric heating causes a disturbance to the Pacific/North American (PNA) pattern which brings lower SLP and increased precipitation around the Gulf of Mexico in the winter season of year (+) (Horel and Wallace, 1981; Giannini et al., 2001b). Concurrently, the PNA anomaly is also responsible for a decrease in the North Atlantic trade winds, through a weakening of the Atlantic subtropical high (Nobre and Shukla, 1996). One consequence of this is reduced moisture convergence into the Amazon basin in spring (+), leading to decreased convection (Marengo, 1992; Marengo and Hastenrath, 1993) and a delay in the onset of the rainy season over the northern Amazon (Liebmann and Marengo, 2001; Marengo et al., 2001). Another consequence of the decreased trade winds is a warming of the TNA, leading to an increase in precipitation in spring (+) over the Caribbean (Enfield and Mayer, 1997; Giannini et al., 2001b). However, a higher than average North Atlantic Oscillation (NAO) in the 1980s and 1990s (during our period of study), strengthening the Atlantic trade winds, is thought to have attenuated or cancelled these effects (Giannini et al., 2001a).

4.2. Methodology

To assess RCA's ability to represent key regional anomalies associated with the aforementioned ENSO variability, we follow Ropelewski and Halpert (1987) and develop composite ENSO events for years (0) and (+). We do not consider the years (−) as there are no documented impacts during this period over our regions of interest. We calculate monthly El Niño and La Niña composites for selected years within our period of study, which results in composites Niño (0), Niño (+), Niña (0) and Niña (+).

Table 1. Strong ENSO events in the 1979–2005 period

El Niño	La Niña
1982–1983	
1986–1987	1988–1989
1991–1992	
1997–1998	1998–1999
2002–2003	1999–2000

The resulting metrics are thus defined as

$$NINOA = \overline{NINO} - CLIM, \tag{1}$$

$$NINAA = \overline{NINA} - CLIM, \tag{2}$$

where $\overline{NINO}$ and $\overline{NINA}$ are the basic ENSO composite values of a given variable for a given month, *CLIM* is the climatological average of the same variable for the same month and *NINOA* and *NINAA* are the anomalies of the ENSO composites.

The events chosen for composite means are the ones used by Seth et al. (2007), based on the National Oceanic and Atmospheric Administration (NOAA) Climate Prediction Center's Oceanic Niño Index (ONI). The condition for defining an El Niño (warm) or La Niña (cold) event is a SSTA of $\pm 0.5\,^{\circ}$C relative to the 1971–2000 base period, over the Niño 3.4 region for five overlapping seasons, using the ERSST.v2 data set (Smith and Reynolds, 2004). We choose only the strongest ENSO events to obtain a clear anomaly signal. The relatively mild La Niña of 1984–1985 has been excluded because the precipitation anomalies are opposed to other La Niña events in the NAMZ and MEX regions. Figure 10d shows the corresponding SSTAs and Table 1 gives the strong ENSO events with corresponding years (0) and (+).

We first analyse spatial maps of SLP, 925 hPa wind, geopotential height and wind at 250 hPa and precipitation anomalies for seasons JAS(0) and JFM(+) to evaluate the simulated large-scale anomalies. Second, we plot annual cycle time-series of spatially averaged precipitation anomalies over the land points of each of the chosen regions (CAR, CAM, NAMZ and MEX) to verify if the known regional anomalies are accurately simulated. We apply a 3-month running mean to the monthly anomalies to highlight seasonal timescales. A final analysis of precipitation variability is done using a multiyear time-series of spatially meaned anomalies, to determine if the model reproduces regional variability associated with different ENSO events.

4.3. Results

4.3.1. Seasonal averages. The important periods of precipitation anomalies associated with ENSO are respectively July–October (0) for CAR and CAM, July (0)–March (+) for NAMZ
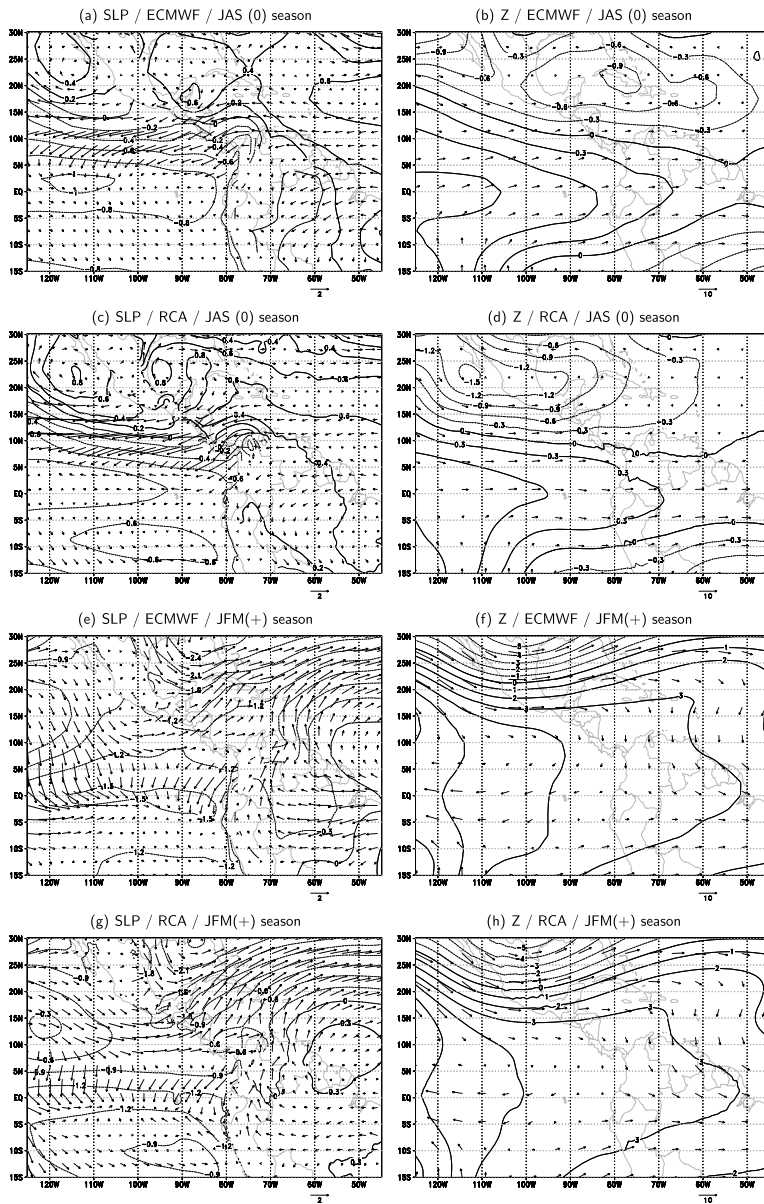
(a) SLP / ECMWF / JAS (0) season

(b) Z / ECMWF / JAS (0) season

(c) SLP / RCA / JAS (0) season

(d) Z / RCA / JAS (0) season

(e) SLP / ECMWF / JFM(+) season

(f) Z / ECMWF / JFM(+) season

(g) SLP / RCA / JFM(+) season

(h) Z / RCA / JFM(+) season

Fig. 6. El Niño anomalies (*NINOA*) of SLP (contours in hPa) and 925 hPa winds (vectors in m s^{-1}) in left-hand column, 250 hPa geopotential height (contours in dam) and winds (vectors in m s^{-1}) in right-hand column. Full lines indicate positive anomalies and dotted lines indicate negative anomalies. The scale of the wind vectors is indicated on each figure.

and October (0)–March (+) for MEX (see Section 4.1). The following section deals only with seasons JAS(0) and JFM(+) which capture the majority of these anomaly periods. Figure 6 shows the NINOA for SLP and 925 hPa wind and 250 hPa geopotential height and wind field, for both ECMWF and RCA. To show the impact on precipitation, we plot the El Niño anomalies (NINOA) for GPCP, CRU, ECMWF and RCA in Fig. 7.

For composite El Niño conditions JAS(0) is when warm SSTAs first appear in the eastern tropical Pacific, while there is a weak cold anomaly in the TNA. The model responds accordingly, with anomalous low pressure and convergence (Fig. 6c) in the lower levels and increased convection and precipitation (Fig. 7g) over the area of positive SSTAs (eastern tropical Pacific), in general accordance with ECMWF SLP and

wind anomalies and GPCP precipitation. This anomalous convection modifies the position of the Walker Cell and strengthens the local Hadley Cell, causing increased subsidence over the Caribbean, Mexico and northern South America, east of the Andes. This can be seen in the upper levels through anomalies in the geopotential height (positive over the eastern tropical Pacific and negative over the Caribbean) and anomalous westerly upper-level winds at the equator. The resulting dry anomaly over northeast South America is correctly simulated (Fig. 7g).

ECMWF SLP anomalies indicate weak anticyclonic anomalies both east and west of Mexico in JAS(0), which reduce moisture convergence over the continent and onto the east and southwest coasts of Mexico. JAS(0) precipitation anomalies in this region (Caribbean and Mexico), while of the correct sign, are
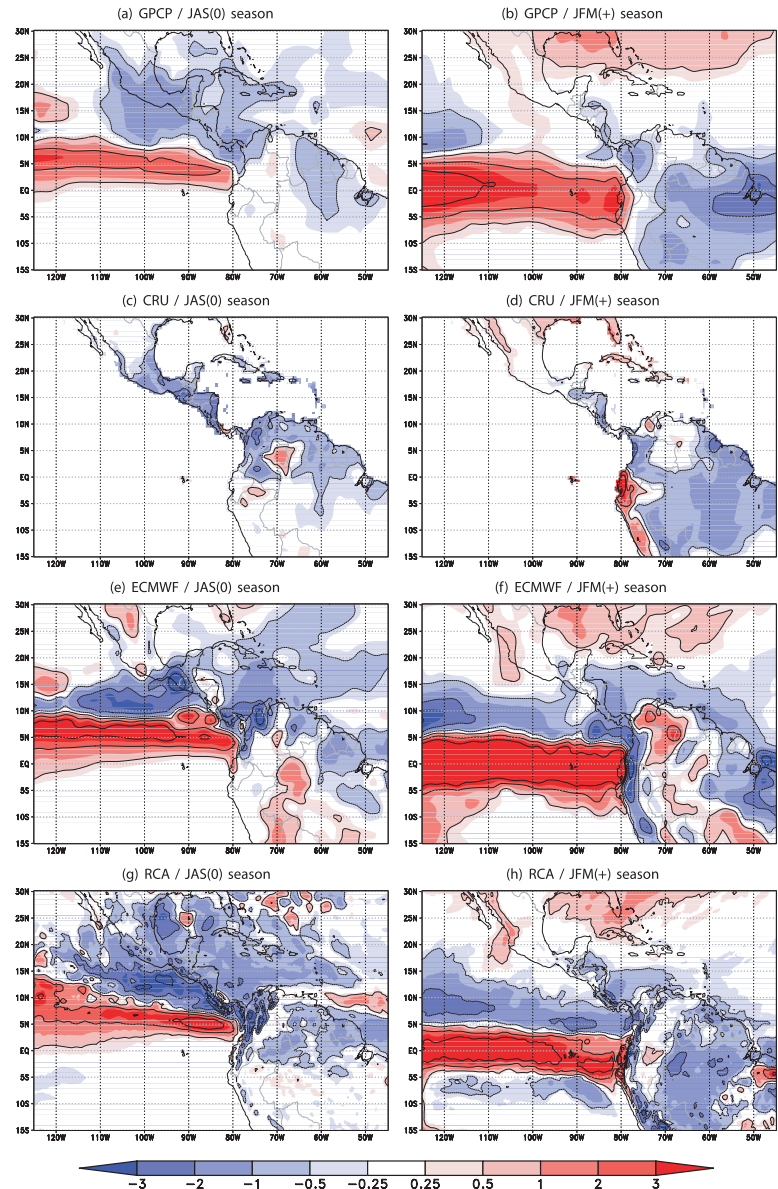
Fig. 7. El Niño anomalies (*NINOA*) of precipitation (mm d^{-1}) seasons JAS(0) and JFM(+) (columns)/GPCP, CRU, ECMWF and RCA (rows).

excessively dry in RCA (mostly over the Gulf of Mexico as seen in Fig. 7, left-hand column). The corresponding SLP and low-level wind field anomalies in RCA are also slightly more intense than seen in ECMWF, consistent with an excess decrease in low-level moisture convergence (and precipitation) over these areas. Furthermore, the 250 hPa geopotential height anomalies in RCA are excessive and displaced somewhat to the west. It appears that the Kain–Fritsch convection scheme in RCA is too responsive to anomalous subsidence in this region, which is part of the descending branch of the Hadley Cell. In this region of anomalous subsidence, model convection appears to completely shut down, whereas in reality it is likely that sporadic weak convection still occurs. As a result, the simulated negative precipitation anomaly is larger than observed.

Season JFM(+) is when the PNA pattern disturbance – initiated in the OND(0) season – spreads southeastward, influencing most of the northern part of the domain, with anomalously low SLP values. Wind patterns shift dramatically (Figs 6e and g), with reduced Atlantic easterly trade winds, leading to reduced evaporation and relatively warmer SSTs over the Caribbean. The PNA anomalies can be clearly seen in the negative 250 hPa geopotential height anomalies (Figs 6f and h) and strengthening of the subtropical jet in the northern portion of the RCA domain in JFM(+) and are in very good agreement with ECMWF anomalies. A widespread wet anomaly north of ≈20°N is well captured in the model (Fig. 7, right-hand column) and linked to the southward influence of the PNA forcing. Over Central America, the RCA simulated negative anomalies are comparable
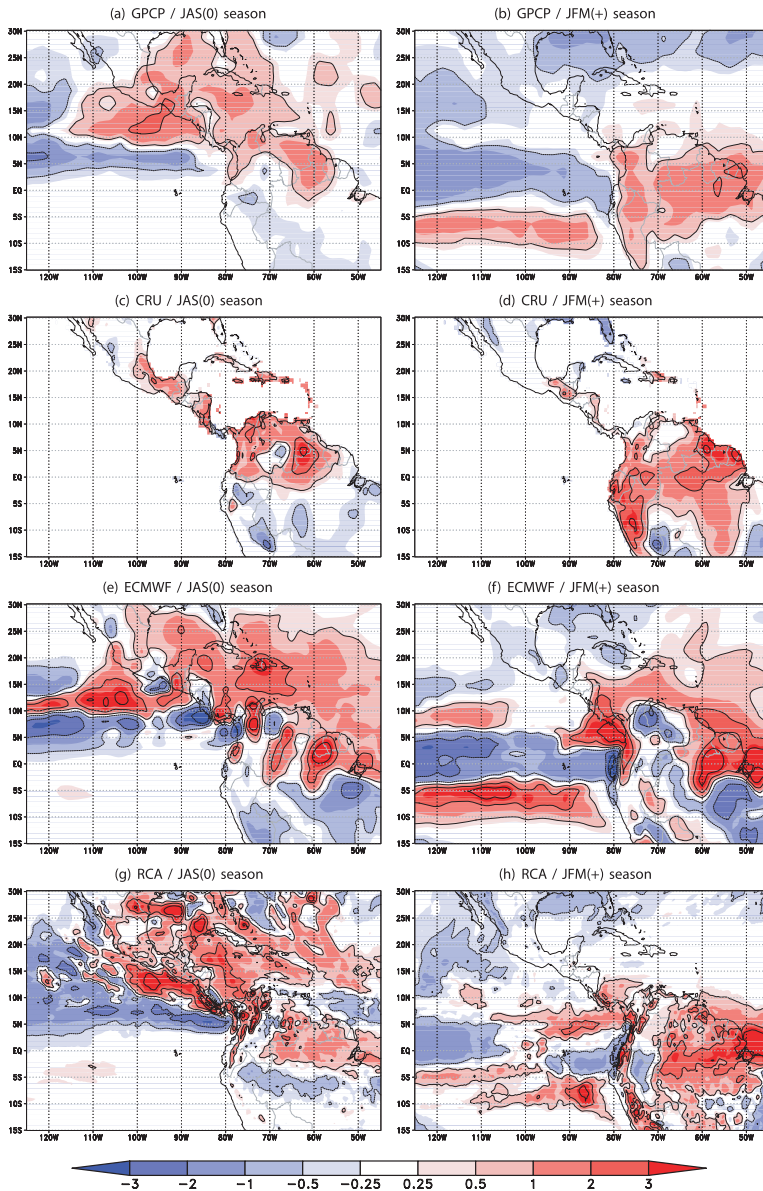
Fig. 8. As Fig. 7 but La Niña anomalies (*NINAA*) of precipitation (mm d^{-1}).

to observations. Most of South America in the model domain is under the influence of decreased easterlies which reduces moisture convergence leading to a dry precipitation anomaly in both the observations and model, whereas ECMWF precipitation suggests a widespread wet anomaly. In JFM(+) season, the CRU observations indicate a thin positive precipitation anomaly along the coast of Ecuador, Peru and northern Chile. This small-scale feature is reasonably captured in the RCA results.

In this section, we discuss La Niña precipitation anomalies (NINAA), for seasons JAS(0) and JFM(+), shown in Fig. 8. This is done to verify if the model can simulate the opposite signed precipitation anomalies associated with La Niña SSTAs. Figures 8a and e indicate a weaker east Pacific ITCZ in JAS(0) accompanied by a weaker descending branch of the Hadley Cell

over the Caribbean, and of the Walker Circulation over northeastern South America. This results in positive precipitation anomalies in these two regions in JAS(0), both of which are relatively well captured by RCA. Wet anomalies in the Caribbean are of comparable magnitude in RCA compared to observations. The MEX region and Gulf of Mexico are excessively wet in RCA in season JAS(0), analogous, in a reverse sense, to the excessive dryness in season JAS(0) of the El Niño composites (Fig. 7g). Here, the convection scheme may be too responsive to reduced climatological subsidence, triggering excessively strong convection in an environment only slightly more supportive of convection. The South American continent is well simulated, with dry conditions south of 5°S and wet conditions to the north.
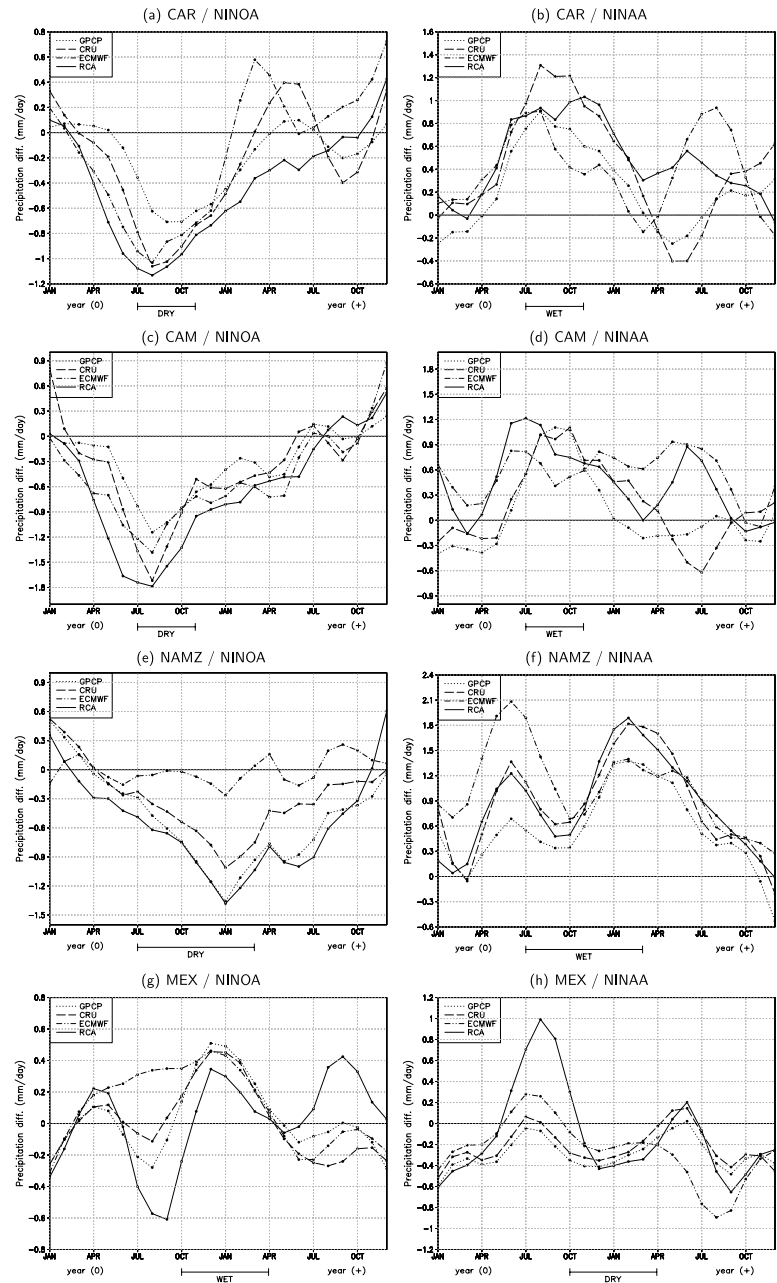
Fig. 9. El Niño (left-hand column) and La Niña (right-hand column) anomalies of precipitation (mm d^{-1}) over land, annual cycle by region. The typical period and impact (wet/dry) of ENSO variability for each region is indicated on the *x*-axis. The scales on the *y*-axis are different in each plot.

In season JFM(+), the model underestimates a dry anomaly along the east Pacific ITCZ. Dry conditions prevail over most of Mexico and the Gulf of Mexico (the reverse of PNA-induced wet conditions in the El Niño composites) and are generally well simulated (note that the absolute magnitude of the anomaly is very small). The Caribbean Sea and TNA are under the influence of a PNA-induced high-pressure anomaly in JFM(+) which causes an increase of the easterly trade winds, with an increase in moisture convergence and precipitation over the Amazon (Marengo, 1992). RCA generally simulates this increase in precipitation over northeast South America. As in the El Niño

JAS(+) anomalies, ECMWF shows opposite signed anomalies to those observed in some parts of South America. It is worth noting that RCA receives its LBCs from the ERA-40/ECMWF analysis. Hence, this improvement in the precipitation anomaly field should be seen as a clear local improvement through dynamical downscaling.

4.3.2. Annual cycle. To assess the time evolution of simulated ENSO anomalies over the four regions of interest, we present, in Fig. 9, 3-month running mean time-series of precipitation anomalies separately for El Niño (left-hand column) and La Niña (right-hand column) composite conditions (obtained as

averages across the years given in Table 1). On the *x*-axis of the figures, we indicate the generally accepted time periods, within the annual cycle, of El Niño and La Niña forced precipitation anomalies (dry/wet) over each region.

In CAM (*typically dry/wet anomalies for El Niño/La Niña composites from July to October (0)*) RCA correctly simulates a dry anomaly from May (0) to May (+) in the El Niño composite (although of slightly excessive magnitude in May–June (0)). A similar, reverse behaviour is seen in the La Niña composites. After November (0) the agreement between all data sets becomes weaker, particularly for the La Niña composites where the anomalies are small and RCA is not able to match observations. It should be borne in mind that there are no consistent and documented ENSO forced anomalies in this period and region. In the broader CAR region ('typically dry/wet from July to October (0)'), the dry anomaly from May (0) to March (+) under El Niño conditions is well simulated in RCA, with a slight dry bias from January to July (+). In the La Niña composites, the simulations are generally of opposite sign to the El Niño anomalies and are accurately simulated until February (+), after which none of the four data sets agree on the anomaly sign.

Over the NAMZ region (*typically dry/wet from July to March (0)*) El Niño conditions are associated with dry anomalies throughout most of the 2 yr composite. As early as May (0) there are dry anomalies (the strongest anomalies being in December (0)–February (+)), and the model is nearly always within the observational range. The ECMWF precipitation fails completely to capture the negative anomaly over NAMZ. As the rainy season in the northern Amazon is normally from February to July, this dry anomaly in El Niño years can be associated with a delay in the onset of the rainy season in year (+). This has been confirmed in a number of earlier studies (Liebmann and Marengo, 2001; Marengo et al., 2001) and will be addressed in TJ2009b using pentad precipitation data. The La Niña composites show practically the opposite anomaly structure to El Niño conditions, with prevailing wet anomalies peaking in January–February (+). This anomaly pattern is also extremely accurate in the RCA results, with the ECMWF anomaly again being an outlier. Analogous to El Niño composites, this wet anomaly is associated with an early onset of the rainy season.

The MEX region (*typically wet/dry from October (0) to March (+)*) is primarily influenced by the PNA pattern. The El Niño composites show a wet anomaly from November (0) to April (+) in the observations. The dry bias in the model in this region results in a weaker and shorter wet period than observed. After this wet period the observations disagree and there is no documented ENSO anomaly pattern. The La Niña composite anomalies are of smaller magnitude in the winter. RCA exhibits excessive magnitude of both the El Niño (negative) and La Niña (positive) anomalies over MEX, consistent with the excessive dry/wet anomalies respectively discussed in the previous section.
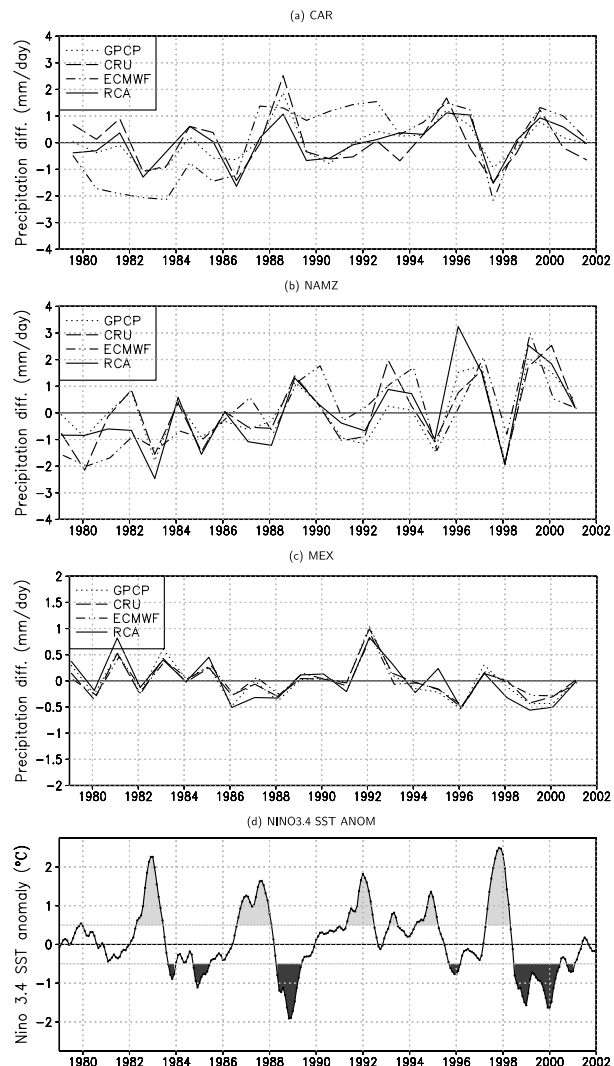

Fig. 10. Time-series of precipitation anomalies over land (mm d^{-1})/ regions (a) CAR(season JAS), (b) NAMZ(season JFM) and (c) MEX(season JFM); (d) Niño 3.4 SST anomaly (°C).

4.3.3. Seasonal anomaly time-series. To evaluate the simulated variability between different ENSO events, we plot in Fig. 10 a time-series of precipitation anomalies over land for all years. For the regions CAR, NAMZ and MEX, we show the interannual variability of precipitation for a single season. The selected seasons (*JAS for CAR and JFM for NAMZ and MEX*) are chosen based on the seasons of largest anomalies in the ENSO composites. Figure 10d shows 3 months running mean anomalies of the ERSST.v2 data set in the Niño 3.4 region, with base climatology from 1971 to 2000 and identifies the ENSO events (El Niño in light grey, La Niña in dark grey).

The response in precipitation anomalies is not a simple function of the magnitude of SSTAs in the tropical east Pacific. Moreover, regional consequences of ENSO are not always consistent with 'canonical' ENSO events (represented by the composites),

Table 2. Linear correlation (RCA vs. observations and ECMWF vs. observations) of seasonal anomalies of precipitation over land

Region	Obs.	RCA		ECMWF	
		All	ENSO	All	ENSO
CAM	GPCP	0.51	(0.75)	0.50	(0.64)
	CRU	**0.65**	0.84	**0.66**	0.82
CAR	GPCP	**0.84**	**0.90**	**0.68**	0.83
	CRU	**0.76**	**0.92**	(0.37)	0.76
MEX	GPCP	**0.90**	**0.97**	**0.96**	**0.99**
	CRU	**0.88**	**0.97**	**0.97**	**0.99**
NAMZ	GPCP	**0.88**	**0.98**	**0.64**	0.86
	CRU	**0.82**	**0.96**	**0.70**	(0.73)

Bold values are significant at 99% level, others at 95% level (except those in parentheses).

in accordance with results from Sardeshmukh et al. (2000). As an example, in the 1984–1985 La Niña event, conditions in JFM(+) are contrary to the composite La Niña anomalies (e.g. dry in NAMZ where the composites show wet). In addition, the 1997–1998 El Niño does not conform to the composite anomalies in the MEX region, while it is very representative in other areas. The model generally agrees with observations and captures the variability between the different ENSO events across the different regions. ECMWF is a clear outlier in regions CAR and NAMZ.

Linear correlations (Pearson correlation coefficient) in time between RCA and the two observational time-series are shown in Table 2, for all years and for strong ENSO years only (defined in Table 1). The MEX region is particularly well correlated for all years, whereas in the CAM region correlation is the lowest and generally not statistically significant. Correlations between RCA and ECMWF are much lower (except in MEX) and are not shown. The correlation for the strong ENSO years is higher than for all years and is greater than 90% in all regions except CAM. This indicates increased predictability during years of strong ENSO forcing. To assess the added value of dynamical downscaling, we also show the correlation between ECMWF and the observations. The correlations are smaller or very close to those between RCA and the observations, except in MEX where more observational data are likely included in the assimilation process of ECMWF. We conclude that where there is a relatively small amount of local data included in the ECMWF assimilation system, RCA has a better performance than ECMWF in terms of simulating year-to-year precipitation variability.

4.3.4. Discussion. The use of composite ENSO events has allowed us to evaluate the average performance of an RCM in simulating regional-scale, seasonal mean anomalies associated with ENSO when forced by observed SSTs and analysed LBCs. This is a first-order evaluation of the ability of an RCM

to downscale large-scale circulation anomalies over the tropical Americas. The model generally captures the sign of the precipitation anomalies in the important seasons, although a few regions of inaccuracy do exist. The most problematic area is the Caribbean and Gulf of Mexico in the JAS(0) season when RCA overestimates the El Niño related dry anomaly and conversely overestimates the wet anomaly in this region in La Niña periods. The Kain–Fritsch convection scheme appears excessively responsive to small changes in large-scale subsidence. During (anomalous) periods of weak, large-scale subsidence (generally not supportive of deep convection), simulated convection essentially shuts down. Conversely during (anomalous) periods of weak, large-scale ascent (generally supportive of deep convection), model convection increases dramatically. We believe this binary response of model convection to changes in large-scale subsidence is much greater than in the real world and is the primary cause of the excess anomalies in this region. In the NAMZ region, the model is very accurate except for a small dry bias in January–March (+), which is just before the rainy season of year (0). This could potentially lead to errors in the prediction of the onset of the rainy season, which exhibits sensitivity to ENSO forcing. The MEX region shows a small dry bias at the end of the rainy season of year (0) and during the winter (+).

By looking at the seasonal anomalies for the different years of the integration, we have established that (1) there is large variability amongst different ENSO events; (2) RCA is able to capture most of this variability; (3) some ENSO events do not correspond to the 'canonical' events as represented by the composites.

5. Assessing the benefits of increased resolution

The potential added value of using a high-resolution climate model is difficult to assess, especially in tropical regions where reliable high-resolution observations are scarce. To make a preliminary estimate of the benefits of increased model resolution, we ran RCA at a lower resolution of 1° (named here RCA1) using the same model domain and boundary conditions. We compare both runs to GPCP and TRMM for the 1998–2005 period. The shorter time period is used ito compare the model precipitation against the higher-resolution TRMM observations. In Fig. 11, we show the climatological average of seasons JFM and JAS. The finer detail, high-intensity precipitation simulated by RCA in the Pacific ITCZ is consistent with the TRMM observations. Similarly, regional-scale details in precipitation associated with variable orography over South America are seen in TRMM and RCA, but are absent in the lower-resolution data sets such as GPCP. When spatially averaged over a larger region GPCP and TRMM are very similar (not shown), however TRMM and RCA do both show increased detail and localized intensity maxima. Finally, the lower-resolution RCA1 reproduces the general spatial patterns of precipitation but shows excessive maxima (compared to the higher-resolution RCA), particularly over northern
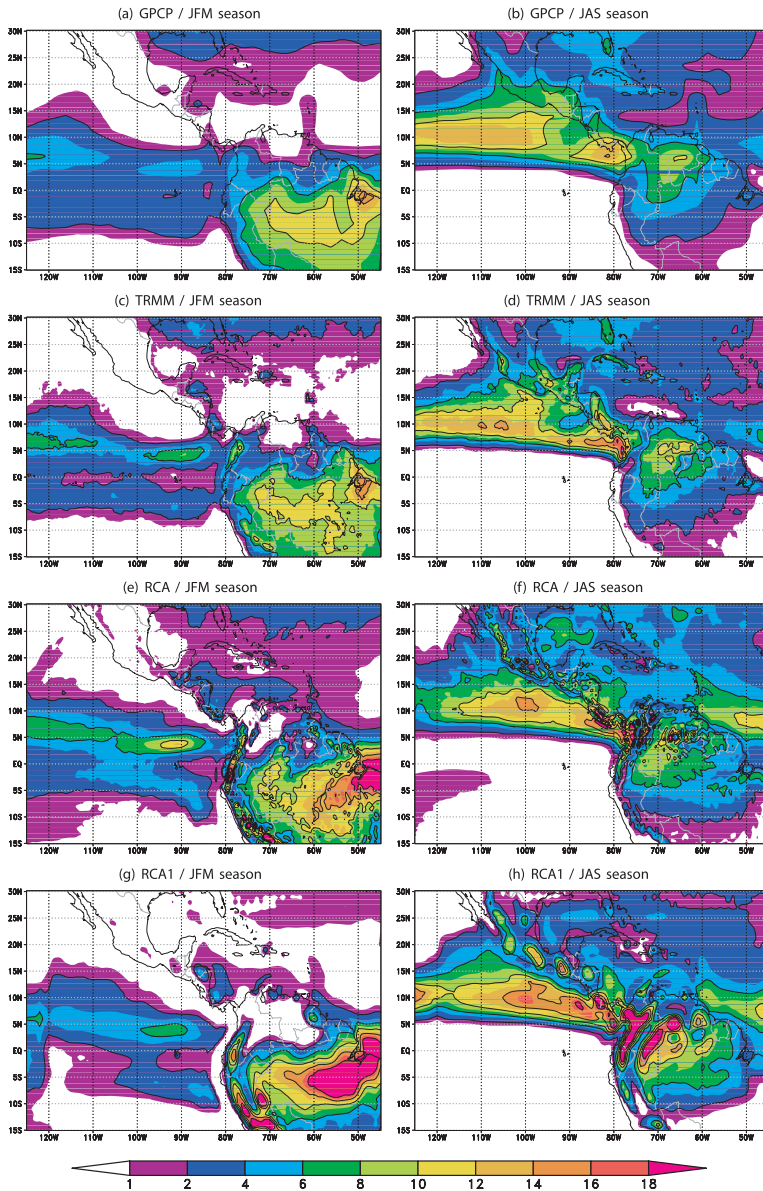
South America and regions of orographic forcing. Examination of the individual resolved and convective precipitation components (not shown) indicates that the primary cause of increased precipitation in RCA1 is associated with excessive triggering of convection over the more widespread/smoother orography in RCA1. In the Rossby Centre model semi-lagrangian dynamics a 1-2-1 filter is applied to the orography field to maintain numerical accuracy at long time steps. This acts to extend the spatial influence of orography on the resolved dynamics in RCA1 (of lower resolution) compared to RCA (of higher resolution). Upward directed, lower tropospheric vertical velocities (as frequently simulated on the upslope of mountains in numerical models employing terrain-following coordinates) can then play an important role in allowing frequent convection in these re-

gions through its role in the Kain–Fritsch trigger function (Kain and Fritsch, 1993).

As the 1998–2005 period is rather short and contains few ENSO events, we use a single ENSO event to assess the benefits of increased resolution in RCA with respect to downscaling regional precipitation anomalies. We show here the 1999–2000 La Niña event because it is the most 'canonical' ENSO event during the available period. Figure 12 shows the precipitation anomaly (NINAA) during the JAS(0) and JFM(+) seasons of the said La Niña event. RCA shows increased (subregional) detail when compared to RCA1 and is also more accurate in several regions. Improvements in JAS(0) are seen in the Caribbean Sea (where RCA1 shows mostly positive anomalies), in northern South America (specifically east of the Andes where there are
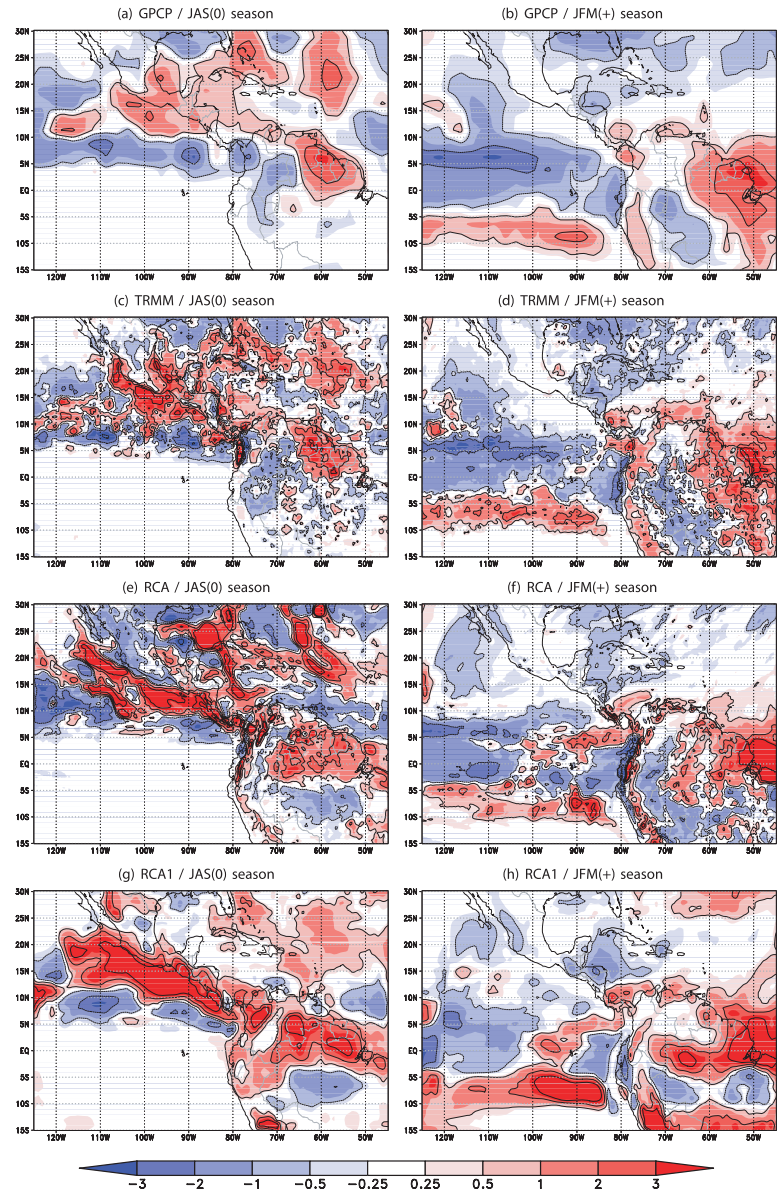
Fig. 12. Precipitation anomaly (mm d^{-1}) during the 1999–2000 La Niña/seasons JAS(0) and JFM(+) (columns)/GPCP, TRMM, RCA and RCA1 (rows).

negative anomalies in the TRMM observations) and in northern Mexico. In season JFM(+), RCA shows increased accuracy in areas surrounding the northern Andes, notably a negative anomaly on the eastern slopes is poorly captured by RCA1. Nevertheless, RCA1 does capture the majority of wet anomalies in CAR, CAM and NAMZ regions during the La Niña event. These results do suggest that a GCM run at a resolution of ≈1° could provide a reasonable amount of regional detail in support of local planning activities.

6. Conclusions

When forced by observed SSTs and analysed lateral boundary conditions RCA is able to (1) simulate with reasonable accu-
racy the climatological annual cycle of precipitation over the tropical east Pacific and distinct regions of Central and South America; (2) capture most of the regional-scale seasonal mean precipitation anomalies over the tropical Americas associated with ENSO forcing; (3) capture the variability between different ENSO events. Moreover, the large-scale anomalies in SLP and low-level winds that are integrally related with the precipitation anomalies, are also well represented by the model. Simulated climatological precipitation over northern Amazon exhibits a wet bias and an erroneous secondary rainfall maximum in December. Modifications to the convection scheme appear necessary to reduce an overestimate of the precipitation anomalies in some regions (e.g. Central America), associated with an oversensitivity to anomalous large-scale vertical velocities. Nevertheless,

the simulated precipitation variability related to ENSO forcing appears quite realistic and supports the use of this RCM for future studies into regional climate variability over the tropical Americas. A companion paper (TJ2009b) looks at the ability of RCA to simulate subseasonal precipitation anomalies associated with ENSO. In future work, we plan to repeat this exercise forcing RCA with boundary conditions from a free-running GCM. This will aid in determining the contribution of local (east Pacific) SST forcing versus more remote forcing, as defined by the RCM lateral boundary conditions, in determining interannual precipitation variability over the tropical Americas.

7. Acknowledgments

References

Aceituno, P. 1988. On the functioning of the southern oscillation in the South American sector. Part I: Surface climate. *Mon. Wea. Rev.* **116**, 505–524.

Adams, D. K. and Comrie, A. C. 1997. The North American Monsoon. *Bull. Am. Meteorol. Soc.* **78**, 2197–2213.

Adler, R. F., Huffman, G. J., Chang, A., Ferraro, R., Xie, P.-P. and co-authors. 2003. The Version-2 Global Precipitation Climatology Project (GPCP) Monthly Precipitation Analysis (1979-Present). *J. Hydrometeorol.* **4**, 1147–1167.

Albrecht, B. A. 1981. Parameterization of trade-cumulus cloud amounts. *J. Atmos. Sci.* **38**, 97–105.

Alexander, M. A., Blade, I., Newman, M., Lanzante, J. R., Lau, N.-C. and co-authors. 2002. The Atmospheric Bridge: the influence of ENSO teleconnections on air-sea interaction over the global oceans. *J. Clim.* **15**, 2205–2231.

Alfaro, E. J. 2002. Some characteristics of the snnual precipitation cycle in Central America and their relationships with its surrounding tropical oceans. *Top. Meteorol. Oceanogr.* **9**, 88–103.

Chiang, J. C. H., Kushnir, Y. and Zebiak, S. E. 2000. Interdecadal changes in eastern Pacific ITCZ variability and its influence on the Atlantic ITCZ. *Geophys. Res. Lett.* **27**, 3687–3690.

Chou, S. C., Bustamante, J. F. and Gomes, J. L. 2005. Evaluation of Eta Model seasonal precipitation forecasts over South America. *Nonlinear Processes Geophys.* **12**, 537–555.

Cuxart, J., Bougeault, P. and Redelsperger, J.-L. 2000. A turbulence scheme allowing for mesoscale and large-eddy simulations. *Quart. J. R. Meteorol. Soc.* **126**, 1–30.

Davies, H. C. 1976. A lateral boundary formulation for multi-level prediction models. *Quart. J. R. Meteorol. Soc.* **102**, 405–418.

Deng, A., Seaman, N. L. and Kain, J. S. 2003. A shallow-convection parameterization for mesoscale models, part I: submodel description and preliminary applications. *J. Atmos. Sci.* **60**, 34–56.

Enfield, D. B. 1996. Relationship of inter-American rainfall to tropical Atlantic and Pacific SST variability. *Geophys. Res. Lett.* **23**, 3305–3308.

Enfield, D. B. and Alfaro, E. J. 1999. The dependence of Caribbean rainfall on the interaction of the tropical Atlantic and Pacific Oceans. *J. Clim.* **12**, 2093–2103.

Enfield, D. B. and Mayer, D. A. 1997. Tropical Atlantic sea surface temperature variability and its relation to El Niño-Southern Oscillation. *J. Geophys. Res.* **102**, 929–945.

Fernandez, J. P. R., Franchito, S. H. and Rao, V. B. 2006a. Simulation of the summer circulation over South America by two regional climate models. Part I: Mean climatology. *Theor. Appl. Climatol.* **86**, 247–260.

Fernandez, J. P. R., Franchito, S. H. and Rao, V. B. 2006b. Simulation of the summer circulation over South America by two regional climate models. Part II: A comparison between 1997/1998 El Niño and 1998/1999 La Niña events. *Theor. Appl. Climatol.* **86**, 261–270.

Giannini, A., Kushnir, Y. and Cane, M. A. 2000. Interannual variability of Caribbean Rainfall, ENSO, and the Atlantic Ocean. *J. Clim.* **13**, 297–311.

Giannini, A., Cane, M. A. and Kushnir, Y. 2001a. Interdecadal changes in the ENSO teleconnection to the Caribbean region and the North Atlantic Oscillation. *J. Clim.* **14**, 2867–2879.

Giannini, A., Chiang, J. C. H., Cane, M. A., Kushnir, Y. and Seager, R. 2001b. The ENSO teleconnection to the tropical Atlantic Ocean: contributions of the remote and local SSTs to rainfall variability in the tropical Americas. *J. Clim.* **14**, 4530–4544.

Gochis, D. J., Shuttleworth, W. J. and Yang, Z.-L. 2002. Sensitivity of the modeled North American Monsoon regional climate to convective parameterization. *Mon. Wea. Rev.* **130**, 1282–1298.

Goddard, L., Mason, S. J., Zebiak, S. E., Ropelewski, C., Basher, R. and co-authors. 2001. Current approaches to seasonal to interannual climate predictions. *Int. J. Climatol.* **21**, 1111–1152.

Hernandez, J. L., Srikishen, J., Erickson, D. J., Oglesby, R. and Irwin, D. 2006. A regional climate study of Central America using the MM5 modeling system: results and comparison to observations. *Int. J. Climatol.* **26**, 2161–2179.

Horel, J. D. and Wallace, J. M. 1981. Planetary-scale atmospheric phenomena associated with the Southern Oscillation. *Mon. Wea. Rev.* **109**, 813–829.

Huffman, G. J., Adler, R. F., Bolvin, D. T., Gu, G., Nelkin, E. J. and co-authors. 2007. The TRMM Multisatellite Precipitation Analysis (TMPA): quasi-global, multiyear, combined-sensor precipitation estimates at fine scales. *J. Hydrometeorol.* **8**, 38–55.

Jones, C. G., Willén, U., Ullerstig, A. and Hansson, U. 2004. The Rossby Centre Regional Atmospheric Climate Model part I: model climatology and performance for the present climate over Europe. *Ambio* **33**, 199–210.

Kain, J. S. 2004. The Kain-Fritsch convective parameterization: an update. *J. Appl. Meteorol.* **43**, 170–181.

Kain, J. S. and Fritsch, J. M. 1990. A one-dimensional entraining/detraining plume model and its application in convective parameterization. *J. Atmos. Sci.* **47**, 2784–2802.

Kain, J. S. and Fritsch, J. M. 1993. Convective parameterizations for Mesoscale Models: the Kain-Fritsch scheme. In: *The representation*

of cumulus convection in numerical models, *Meteor. Monogr.* Volume 46. American Meteorological Society, 165–170.

Kjellström, E., Bärring, L., Gollvik, S., Hansson, U., Jones, C. and co-authors. 2005. A 140-year simulation of European climate with the new version of the Rossby Centre regional atmospheric climate model (RCA3). *SMHI Reports Meteorology and Climatology* (108). SMHI, SE-60176 Norrköping, Sweden, 54 pp.

Kousky, V. E., Kagano, M. T. and Cavalcanti, I. 1984. A review of the Southern Oscillation: oceanic-atmospheric circulation changes and related rainfall anomalies. *Tellus A* **36A**, 490–504.

Latif, M., Anderson, D., Barnett, T., Cane, M., Kleeman, R. and co-authors. 1998. A review of the predictability and prediction of ENSO. *J. Geophys. Res.* **103**, 14 375–14 393.

Lenderink, G. and Holtslag, A. A. M. 2004. An updated length-scale formulation for turbulent mixing in clear and cloudy boundary layers. *Quart. J. R. Meteorol. Soc.* **130**, 3405–3427.

Liebmann, B. and Marengo, J. A. 2001. Interannual variability of the rainy season and rainfall in the Brazilian Amazon Basin. *J. Clim.* **14**, 4308–4318.

Magaña, V. and Caetano, E. 2005. Temporal evolution of summer convective activity over the Americas warm pools. *Geophys. Res. Lett.* **32**, L02803.

Magaña, V., Amador, J. A. and Medina, S. 1999. The midsummer drought over Mexico and Central America. *J. Clim.* **12**, 1577–1588.

Magaña, V. O., Vázquez, J. L., Pérez, J. L. and Pérez, J. B. 2003. Impact of El Niño on precipitation in Mexico. *Geofis. Int.* **42**, 313–330.

Marengo, J. A. 1992. Interannual variability of surface climate in the Amazon basin. *Int. J. Climatol.* **12**, 853–863.

Marengo, J. A. and Hastenrath, S. 1993. Case studies of extreme climatic events in the Amazon Basin. *J. Clim.* **6**, 617–627.

Marengo, J. A., Liebmann, B., Kousky, V. E., Filizola, N. P. and Wainer, I. C. 2001. Onset and end of the rainy season in the Brazilian Amazon Basin. *J. Clim.* **14**, 833–852.

Marengo, J., Cavalcanti, I., Satyamurty, P., Trosnikov, I., Nobre, C. and co-authors. 2003. Assessment of regional seasonal rainfall predictability using the CPTEC/COLA atmospheric GCM. *Clim. Dyn.* **21**, 459–475.

Masson, V., Champeaux, J.-L., Chauvin, F., Meriguet, C. and Lacaze, R. 2003. A global database of land surface parameters at 1-km resolution in meteorological and climate models. *J. Clim.* **16**, 1261–1282.

Mitchell, T. D. and Jones, P. D. 2005. An improved method of constructing a database of monthly climate observations and associated high-resolution grids. *Int. J. Climatol.* **25**, 693–712.

Nobre, P. and Shukla, J. 1996. Variations of sea surface temperature, wind stress, and rainfall over the tropical Atlantic and South America. *J. Clim.* **9**, 2464–2479.

Onogi, K., Tsutsui, J., Koide, H., Sakamoto, M., Kobayashi, S. and co-authors. 2007. The JRA-25 reanalysis. *J. Meteorol. Soc. Jpn.* **85**, 369–432.

Palmer, T. N., Alessandri, A., Andersen, U., Cantelaube, P., Davey, M. and co-authors. 2004. Development of a European multi-model ensemble system for seasonal to inter-annual prediction (DEMETER). *Bull. Am. Meteorol. Soc.* **85**, 853–872.

Pan, Z., Takle, E., Gutowski, W. and Turner, R. 1999. Long simulation of Regional Climate as a Sequence of Short Segments. *Mon. Wea. Rev.* **127**, 308–321.

Philander, S. G. 1990. *El Niño, La Niña, and the Southern Oscillation, International Geophysics Series* Volume 46 (eds. R. Dmowska, and J. R. Holton) Academic Press, San Diego, CA.

Qian, J.-H., Seth, A. and Zebiak, S. 2003. Reinitialized versus continuous simulations for regional climate downscaling. *Mon. Wea. Rev.* **131**, 2857–2874.

Räisänen, P., Rummukainen, M. and Räisänen, J. 2000. Modification of the HIRLAM radiation scheme for use in the Rossby Centre regional Atmospheric Climate model. *Report 49*, Department of Meteorology, University of Helsinki, 71 pp.

Rasch, P. J. and Kristansson, J. E. 1998. A comparison of the CCM3 model climate using diagnosed and predicted condensate parameterizations. *J. Clim.* **11**, 1587–1614.

Rauscher, S. A., Seth, A., Liebmann, B., Qian, J.-H. and Camargo, S. J. 2007. Regional climate model-simulated timing and character of seasonal rains in South America. *Mon. Wea. Rev.* **135**, 2642–2657.

Ropelewski, C. F. and Halpert, M. S. 1987. Global and regional scale precipitation patterns associated with the El Niño/Southern Oscillation. *Mon. Wea. Rev.* **115**, 1606–1626.

Ropelewski, C. F. and Halpert, M. S. 1989. Precipitation patterns associated with the high index phase of the southern oscillation. *J. Clim.* **2**, 268–284.

Ropelewski, C. F. and Halpert, M. S. 1996. Quantifying southern oscillation-precipitation relationships. *J. Clim.* **9**, 1043–1059.

Samuelsson, P., Gollvik, S. and Ullerstig, A. 2006. The land-surface scheme of the Rossby Centre regional atmospheric climate model (RCA3). *Report in Meteorology 122, SMHI*. SE-601 76 Norrköping, Sweden.

Sardeshmukh, P. D. and Hoskins, B. J. 1988. The generation of global rotational flow by steady idealized tropical divergence. *J. Atmos. Sci.* **45**, 1228–1251.

Sardeshmukh, P. D., Compo, G. P. and Penland, C. 2000. Changes of probability associated with El Niño. *J. Clim.* **13**, 4268–4286.

Savijärvi, H. 1990. Fast radiation parameterisation schemes for mesoscale and short-range forecast models. *J. Appl. Meteorol.* **29**, 437–447.

Seth, A., Rauscher, S. A., Camargo, S. J., Qian, J.-H. and Pal, J. S. 2007. RegCM3 regional climatologies for South America using reanalysis and ECHAM global model driving fields. *Clim. Dyn.* **28**, 461–380.

Shukla, J. 1998. Predictability in the midst of chaos: a scientific basis for climate forecasting. *Science* **282**, 728–731.

Shukla, J., Anderson, J., Baumhefner, D., Brankovic, C., Chang, Y. and co-authors. 2000. Dynamical seasonal prediction. *Bull. Am Meteorol. Soc.* **81**, 2593–2606.

Simmons, A., Wallace, J. and Branstator, G. 1983. Barotropic wave propagation and instability, and atmospheric teleconnection patterns. *J. Atmos. Sci.* **40**, 1363–1392.

Small, R. J. O., de Szoeke, S. P. and Xie, S.-P. 2007. The Central American midsummer drought: regional aspects and large-scale forcing. *J. Clim.* **20**, 4853–4873.

Smith, T. M. and Reynolds, R. W. 2004. Improved extended reconstruction of SST (1854-1997). *J. Clim.* **17**, 2466–2477.

Sun, L., Moncunill, D. F., Li, H., Moura, A. D., Filho, F. D. A. D. S. and co-authors. 2006. An operational dynamical downscaling prediction system for Nordeste Brazil and the 2002-04 real-time forecast evaluation. *J. Clim.* **19**, 1990–2007.

Taylor, M. A. and Alfaro, E. J.. 2005. Climate of Central America and the Caribbean. In: *The Encyclopedia of World Climatology* (ed. J. E. Oliver), Springer, Netherlands, 193–189.

Taylor, M. A., Enfield, D. B. and Chen, A. A. 2002. Influence of the tropical Atlantic versus the tropical Pacific on Caribbean rainfall. *J. Geophys. Res.* **107**, 3127.

Tourigny, E. and Jones, C. 2009. An analysis of regional climate model performance over the tropical Americas. Part II: simulating subseasonal variability of precipitation associated with ENSO forcing. *Tellus A*, doi:10.1111/j.1600-0870.2008.00387.x.

Uppala, S. M., Kållberg, P. W., Simmons, A. J., Andrae, U., da Costa Bechtold, V. and co-authors. 2005. The ERA-40 re-analysis. *Quart. J. R. Meteorol. Soc.* **131**, 2961–3012.

Wang, H.-J., Zhang, R.-H., Cole, J. and Chavez, F. 1999. El Niño and the related phenomenon Southern Oscillation (ENSO): the largest signal in interannual climate variation. *Proc. Natl. Acad. Sci. USA* **96**, 11 071–11 072.

Xie, S.-P., Miyama, T., Wang, Y., Xu, H., de Szoeke, S. P. and co-authors. 2007. A regional ocean-atmosphere model for eastern pacific climate: toward reducing tropical biases. *J. Clim.* **20**, 1504–1522.

Xu, K.-M. and Krueger, S. K. 1991. Evaluation of cloudiness parameterizations using a cumulus ensemble model. *Mon. Wea. Rev.* **119**, 342–367.

Xu, K.-M. and Randall, D. A. 1996. A semiempirical cloudiness parameterization for use in climate models. *J. Atmos. Sci.* **53**, 3084–3102.

Xu, J., Gao, X., Shuttleworth, J., Sorooshian, S. and Small, E. 2004. Model climatology of the North American Monsoon onset period during 1980–2001. *J. Clim.* **17**, 3892–3906.